Title

Assessing cortical bone mechanical properties using collagen proton fraction from ultrashort echo time magnetization transfer (UTE-MT) MRI modeling.

Authors

Jerban, Saeed
Ma, Yajun
Dorthe, Erik W
et al.

Publication Date

2019-12-01

DOI

10.1016/j.bonr.2019.100220

Peer reviewed

Bone Reports 11 (2019) 100220

Contents lists available at ScienceDirect

Bone Reports

journal homepage: www.elsevier.com/locate/bonr

Assessing cortical bone mechanical properties using collagen proton fraction from ultrashort echo time magnetization transfer (UTE-MT) MRI modeling

Saeed Jerban[a], Yajun Ma[a], Erik W. Dorthe[b], Lena Kakos[a], Nicole Le[c], Salem Alenezi[d], Robert L. Sah[e,f], Eric Y. Chang[c,a], Darryl D'Lima[b], Jiang Du[a,*]

[a] Department of Radiology, University of California, San Diego, CA 92093, USA
[b] Shiley Center for Orthopedic Research and Education at Scripps Clinic, La Jolla, CA 92037, USA
[c] Radiology Service, VA San Diego Healthcare System, San Diego, CA 92161, USA
[d] Research and Laboratories Sector, Saudi Food and Drug Authority, Riyadh 3292, Saudi Arabia
[e] Department of Bioengineering, University of California, San Diego, CA 92093, USA
[f] Department of Orthopaedic Surgery, University of California, San Diego, CA 92093, USA

ARTICLE INFO

Keywords:
Cortical bone
MRI
Ultrashort echo time
Mechanical properties
Bone microstructure
Magnetization transfer

ABSTRACT

Cortical bone shows as a signal void when using conventional clinical magnetic resonance imaging (MRI). Ultrashort echo time MRI (UTE-MRI) can acquire high signal from cortical bone, thus enabling quantitative assessments. Magnetization transfer (MT) imaging combined with UTE-MRI can indirectly assess protons in the organic matrix of bone. This study aimed to examine UTE-MT MRI techniques to estimate the mechanical properties of cortical bone. A total of 156 rectangular human cortical bone strips were harvested from the tibial and femoral midshafts of 43 donors (62 ± 22 years old, 62 specimens from females, 94 specimens from males). Bone specimens were scanned using UTE-MT sequences on a clinical 3 T MRI scanner and on a micro-computed tomography (μCT) scanner. A series of MT pulse saturation powers (400°, 600°, 800°) and frequency offsets (2, 5, 10, 20, 50 kHz) was used to measure the macromolecular fraction (MMF) utilizing a two-pool MT model. Failure mechanical properties of the bone specimens were measured using 4-point bending tests. MMF from MRI results showed significant strong correlations with cortical bone porosity ($R = -0.72$, $P < 0.01$) and bone mineral density (BMD) ($R = +0.71$, $P < 0.01$). MMF demonstrated significant moderate correlations with Young modulus, yield stress, and ultimate stress ($R = 0.60$–0.61, $P < 0.01$). These results suggest that the two-pool UTE-MT model focusing on the organic matrix of bone can potentially serve as a novel tool to detect the variations of bone mechanical properties and intracortical porosity.

1. Introduction

Clinical assessment of cortical bone focuses mainly on the mineral compartment of bone, measuring bone mineral density (BMD) in patients using x-ray-based techniques. The most commonly employed x-ray-based techniques are dual-energy X-ray absorptiometry (DEXA), quantitative computed tomography (QCT), and high-resolution peripheral quantitative computed tomography (HR-pQCT) (Manhard et al., 2017; Moser et al., 2015).

Recently, magnetic resonance imaging (MRI)-based assessment of cortical bone has received a great deal of attention as it enables investigation into the bone organic matrix, while avoiding potential harm caused by x-ray imaging techniques (Manhard et al., 2017; Du and Bydder, 2013; Chang et al., 2015a; Wehrli, 2013). However, due to bone's very short apparent transverse relaxation time (T2*), clinical MRI is not able to detect considerable signal from cortical bone (Manhard et al., 2017; Du and Bydder, 2013; Chang et al., 2015a; Wehrli, 2013). Ultrashort echo time (UTE)-MRI, on the other hand, can image cortical bone with a high signal (Du and Bydder, 2013; Chang et al., 2015b; Rajapakse et al., 2015; Seifert and Wehrli, 2016; Granke et al., 2015a; Nyman et al., 2008; Manhard et al., 2016; Diaz et al., 2012; Du et al., 2010; Ma et al., 2016a; Manhard et al., 2014; Zhao

Abbreviations: MR, magnetic resonance; MRI, magnetic resonance imaging; 3D, three-dimensional; 3D-UTE, three-dimensional ultrashort echo time imaging; RF, radio frequency; FOV, field of view; MT, magnetization transfer; ROI, region of interest; TE, echo time; TR, repetition time; CT, computed tomography; μCT, micro-computed tomography; MMF, macromolecular proton fraction; T2MM, macromolecular T2; FA, flip angle; BMD, bone mineral density; PBS, phosphate-buffered saline; DEXA, dual-energy X-ray absorptiometry

* Corresponding author at: Department of Radiology, University of California, 9500 Gilman Drive, San Diego, CA 92093, USA.
E-mail address: jiangdu@ucsd.edu (J. Du).

https://doi.org/10.1016/j.bonr.2019.100220
Received 26 July 2019; Accepted 2 August 2019
Available online 02 August 2019

et al., 2017; Nazaran et al., 2017; Jerban et al., 2018; Jerban et al., 2019a; Wan et al., 2019; Lu et al., 2019; Jang et al., 2018; Jerban et al., 2019b; Ma et al., 2019). With UTE-MRI, signal can be acquired after radiofrequency (RF) excitation—as quickly as is allowed by the RF hardware (tens of microseconds or shorter)—before major decay in transverse magnetization. In addition to morphological imaging, UTE-MRI allows for quantitative assessment of cortical bone, including measurement of longitudinal relaxation time (T1), T2*, and water content (Rajapakse et al., 2015; Manhard et al., 2014; Lu et al., 2019; Bae et al., 2012; Tyler et al., 2007; Rad et al., 2011; Abbasi-Rad and Saligheh Rad, 2017; Li et al., 2014; Granke et al., 2015b).

Three major hydrogen proton pools with different T2* values are present in bone: 1) collagen backbone protons, 2) bound water, and 3) pore water and lipid (Du and Bydder, 2013; Seifert and Wehrli, 2016; Horch et al., 2011; Manhard et al., 2015). The associated T2* values for the aforementioned proton pools on a 3 T MR scanner are < 20 μs, 300–400 μs, and > 1 ms, respectively (Du and Bydder, 2013; Chang et al., 2015a; Seifert and Wehrli, 2016). The T2*s of collagen backbone protons are extremely short, making them a challenge to be directly imaged with current MRI scanners (Ma et al., 2016b). Magnetization transfer (MT) imaging combined with UTE-MRI has recently been introduced as a technique to indirectly assess protons in the collagenous matrix (Chang et al., 2015b; Ma et al., 2016a; Jerban et al., 2018; Jerban et al., 2019a; Ma et al., 2017a; Springer et al., 2009). With MT techniques, a high-power saturation RF pulse (such as a Fermi-type pulse) is used with a pre-defined frequency offset from the water protons' resonance frequency to saturate the magnetization of protons in the collagenous matrix. The saturated magnetization transfers from the collagenous matrix to water protons, which can then be imaged with UTE-MRI.

UTE-MT assessment of collagen protons, such as MT ratio (MTR) derived from 2D radial UTE-MT imaging, has been shown to be significantly correlated with bone mechanical properties (Chang et al., 2015b). Higher MTR indicates more transferred saturation to the water pool, implying less water in bone. However, MTR is hardware-dependent and varies significantly between different RF pulse powers and frequency offsets. Moreover, MTR does not provide quantitative information of the macromolecular pool. The magnitude of the transferred saturation correlates with the macromolecular proton fraction (MMF) relative to water protons in the tissue. MMF, as well as macromolecular proton relaxation times and exchange rates, can be obtained using two-pool modeling of UTE-MT data acquired with a series of RF pulse powers and frequency offsets (Ma et al., 2016a; Ma et al., 2017a; Ma et al., 2017b). MMF is assumed to represent the bone matrix volume relative to bone water. Thus, the two-pool UTE-MT technique has the potential to diagnose certain bone diseases associated with porosity variation and bone matrix changes, such as osteoporosis. MMF from UTE-MT modeling has shown strong correlation with human bone microstructure, as measured with micro-computed tomography (μCT) and histomorphometry (Jerban et al., 2019a; Jerban et al., 2019c). Recently, the two-pool UTE-MT technique has been utilized to detect *ex vivo* fibular bone stress injury induced by cyclic loading where the bone collagenous matrix was affected despite an unchanged BMD (Jerban et al., 2018). For diseases which affect the bone collagenous matrix and bone mineral differently, such as osteomalacia (Bhan et al., 2018; Becker, 2005), the two-pool UTE-MT technique can provide information that is complementary to BMD measurements. Nevertheless, the relationship between UTE-MT modeling measures and the failure mechanical properties of cortical bone needs to be determined prior to investigating the clinical performance of UTE-MT modeling methods.

The purpose of this study was to investigate the relationship between the two-pool UTE-MT modeling measurements and mechanical properties of human cortical bone. This study highlights the potential applications of UTE-MT methods for estimating the mechanical properties of cortical bone in the human skeleton. This technique may be useful for more accurate estimation of the fracture risk in patients with osteoporosis.

2. Materials and methods

2.1. Bone strips preparation

Cortical bone specimens were harvested from tibial and femoral midshafts of 43 donors (62 ± 22 years old, 156 total specimens, 62 specimens from females, 94 specimens from males) provided by a nonprofit whole-body donation company (United Tissue Network, Phoenix, AZ). Tibial and femoral midshafts were cut into 40 mm segments using a commercial band saw. After removal of the bone marrow, 1–3 rectangular bone strips approximately 4 mm × 2 mm × 40 mm were harvested from each specimen using a low-speed diamond saw (Isomet 1000, Buehler, IL). All bone specimens were immersed in phosphate-buffered saline (PBS) for twelve hours at room temperature before the MRI scans. Then, specimens were randomly distributed for placement in eight 30-mL syringes (17–20 specimens per syringe) filled with perfluoropolyether (Fomblin, Ausimont, Thorofare, NJ) to minimize dehydration and susceptibility artifacts during MRI scan.

2.2. UTE-MR imaging protocol

The UTE-MRI imaging were performed on a 3 T clinical scanner (GE Healthcare, Waukesha, WI) using an in-house-made 1-in. diameter transmit and receive birdcage coil. There were two quantitative protocols involved in the UTE-MRI scans: First, an actual flip angle imaging variable TR (AFI-VTR) sequence was performed (AFI: TE = 0.032, TRs = 20, and 100 ms; VTR: TE = 0.032; TRs = 20, 40, 100, and 150 ms; FA = 45°) for T1 measurement (Ma et al., 2018), which is the prerequisite for two-pool MT modeling. The scan time for T1 measurement was approximately 40 min. Second, a set of 3D-UTE-Cones-MT sequences (Fermi saturation pulse power = 400°, 600°, and 800°; frequency offset = 2, 5, 10, 20, and 50 kHz; FA = 10°; rectangular RF excitation pulse with a duration of 26 μs; 9 spokes acquired after each MT preparation) was performed for two-pool MT modeling (Ma et al., 2016a; Ma et al., 2017a; Ma et al., 2017b). The total scan time for MT sequences was approximately 30 min. Other imaging parameters included: field of view (FOV) = 40 mm × 40 mm, matrix = 160 × 160, slice thickness = 2 mm, receiver bandwidth = ± 62.5 kHz. Features of the 3D-UTE-Cones sequence have been described in previous studies (Gurney et al., 2006; Carl et al., 2015; Ma et al., 2017c). The details of the two-pool UTE-MT modeling were given in earlier studies by Ma et al. (Ma et al., 2016a; Ma et al., 2017a; Ma et al., 2017b).

2.3. Micro-computed tomography (μCT)

All bone strips were scanned using a Skyscan 1076 (Kontich, Belgium) μCT scanner at 9 μm isotropic voxel size. The total μCT scan time was twelve hours for all 156 specimens. Bone specimens were scanned in the presence of two cylindrical hydroxyapatite phantoms (0.25 and 0.5 g/cm^3) to enable BMD measurements in addition to bone porosity. A 0.05-mm aluminum filter plus a 0.038-mm copper filter were used during the μCT scans. Other scanning parameters were as follows: 100 kV, 100 mA, 0.3° rotation step, and 5 frame-averaging.

2.4. Mechanical failure test

The bone samples were subjected to an incremental bending load session using a 4-point bending setup (ASTM, 2011) for mechanical properties measurement. The jig setup comprised of four tungsten carbide pins (3-mm diameter) held in two machined aluminum seats. The upper aluminum seat connected to the actuator and the lower aluminum seat connected to the load cell. The 4-point bending jig was mounted onto a mechanical testing machine (model 8511.20, Instron, Norwood, MA, USA), including a 4500 N load cell (Sensotec 1000 LBS)

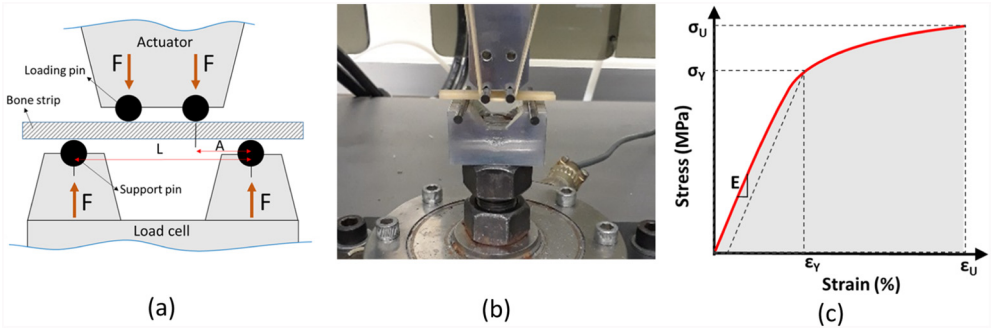

Fig. 1. Standard four-point bending setup to measure the tensile mechanical properties of cortical bone specimens. (a) Schematics of the four-point bending jigs at the longitudinal cross-section (loading and support pins' diameter = 3 mm, L = 24 mm, A = 8 mm; bone strip thickness = approx. 2 mm). The experiments were displacement-controlled at 0.1 mm/s rate when the force was recorded. (b) Prepared bone cortical bone strips (approx. 40 mm length) under mechanical loading using the fabricated four-point bending jigs (aluminum seats and tungsten carbide pins) mounted on an Instron 8511.20 machine. (c) Schematic of the stress–strain curve for calculating mechanical properties such as Young's modulus (E), yield stress (σ_Y), yield strain (ε_Y), ultimate stress (σ_U), ultimate strain (ε_U), and failure energy (W_f).

with an actuator displacement accuracy of < 0.002 mm. The loading protocol was displacement-controlled, while the total force was continuously recorded. The mechanical test involved sensing the contact condition, followed by application of uniaxial displacement of the actuator at 0.1 mm/s until specimen failure. The failure test duration for each sample was between 30 and 60 s. The schematics of the 4-point bending jig and the assembled setup are shown in Fig. 1a and b, respectively.

2.5. Two-pool MT modeling

The acquired MT data with three saturation pulse power levels and five frequencies were fitted using a previously described modified rectangular pulse approximation (mRP) approach (Ma et al., 2016a; Ma et al., 2017a; Ma et al., 2017b). The two-pool MT model estimates MMF and macromolecular T2 ($T2_{MM}$) in cortical bone. In this model, cortical bone is assumed to have two different proton pools. The first pool is the macromolecular proton pool (comprised mainly of collagen backbone protons), which has a very broad spectrum or extremely short T2 (~10 us). The second pool is the water proton pool. The protons of the macromolecular and water pools continuously exchange their magnetizations. Specifically, when the macromolecular proton magnetization is partially saturated using RF excitation with a predefined offset frequency from water spin, the acquired water signal intensity decreases due to the magnetization transfer (Ma et al., 2016a; Ma et al., 2017a; Ma et al., 2017b). All UTE-MRI measurements and models were performed using codes developed in-house in MATLAB.

2.6. Measuring bone porosity and BMD

The μCT images were segmented (distinguish between bone and pores) using a single gray intensity threshold. Gray intensity histograms were used to select the gray intensity threshold for segmentation process. The selected threshold was verified based on the visual inspection of the bone-pore interface in raw μCT images. Bone porosity was estimated as the number of voxels in pores to the total number of voxels covering each bone strip. The diameter of the largest covering sphere was set as the pore size at each pore voxel. Such pore size definition is an oft-used definition for semispherical or ellipsoidal pores in the literature (Hildebrand and Rüegsegger, 1997; Darabi et al., 2007; Bashoor-Zadeh et al., 2010). Local BMD value at each voxel was set as a linear function of its gray intensity, which was derived using the average gray intensity of the scanned hydroxyapatite phantoms with known density (0.25 and 0.75 g/cm^3). Average BMD was calculated for each specimen by averaging the local BMD values over all corresponding voxels.

2.7. Mechanical properties measurement

The stress-strain (σ-ε) relationship for each bone beam during the failure test was determined and depicted as a stress-strain curve by using the measured force and displacement data, as well as the accurately measured sample dimensions from μCT data (Fig. 1c). The stress-strain relationship was calculated for a section in the middle of the beam (between loading pins, Fig. 1a) at the beam's surface, which experiences the highest stress on average. Using the estimated stresses at the surface of the beam based on standard approaches ($\sigma = MC/I$, where σ, M, and I, are stress, the moment at the middle of the beam, and second moment of area of the beam's cross-section, respectively) (Hammant, 1971) was not truly applicable for cortical bone, particularly for porous specimens (Baratta, 1982; ASTM, 2015).

For bone specimens with large pores relative to the bone thickness (*i.e.*, pore/thickness > 15), the routine 4-point bending stress calculation leads to dramatic overestimations (Koudelka et al., 2011), as described in ASTM C1674 for ceramic beams with engineered porosity (ASTM, 2015). ASTM C1674 was used to modify the estimated stresses after measuring the accurate second moment of area of the beam's cross-section (I) using μCT data.

Cortical bone is considered a brittle material, and its mechanical properties depend on the specimens' dimensions (Weibull, 1939; Quinn and Quinn, 2010). Specifically, the effective mechanical stress (σ_{Ef}) on a unit of volume in brittle materials can be estimated using applied stress (σ_{Ap}) on the actual volume (V_{Ap}) and Weibull modulus (m) (*i.e.*, $\frac{\sigma_{Ef}}{\sigma_{Ap}} = \left(\frac{V_{Ap}}{1}\right)^{1/m}$). A Weibull modulus (Weibull, 1939) of four was considered to modify the estimated stresses for the specimen's dimensions. The selected Weibull modulus was in the range of reported values for cortical bone in the literature (Khandaker and Ekwaro-Osire, 2013; Bigley et al., 2008a; Bigley et al., 2008b). It should be noted that lack of bone in older donors led to thinner bone specimens compared with young donors.

After stress modifications and determination of the stress-strain curve (Fig. 1c), the Young's modulus of elasticity (E) was determined from a straight line fit to the initial part of the stress–strain curve. A yield point was defined at a point on the curve where the curve deviated by a strain of 0.002 from the linear part of the curve described by the Young's modulus (ASTM, 2011). The yield point was used to determine both yield stress (σ_Y) and yield strain (ε_Y). The maximum stress and its corresponding strain were assigned to the ultimate stress (σ_U) and ultimate strain (ε_U), respectively. The failure energy or work to failure (W_F) was defined as the area below the stress-strain curve.

2.8. Statistical correlations

UTE-MRI results of one slice from the middle of each bone strip were compared with the average μCT-based measures in the corresponding 220 slices. Then, the MRI and μCT results were both compared with the mechanical properties calculated after failure tests. Finally, Pearson's correlation coefficients were calculated between UTE-MRI measures (T1, MMF, and $T2_{MM}$) and μCT measures (BMD, porosity,

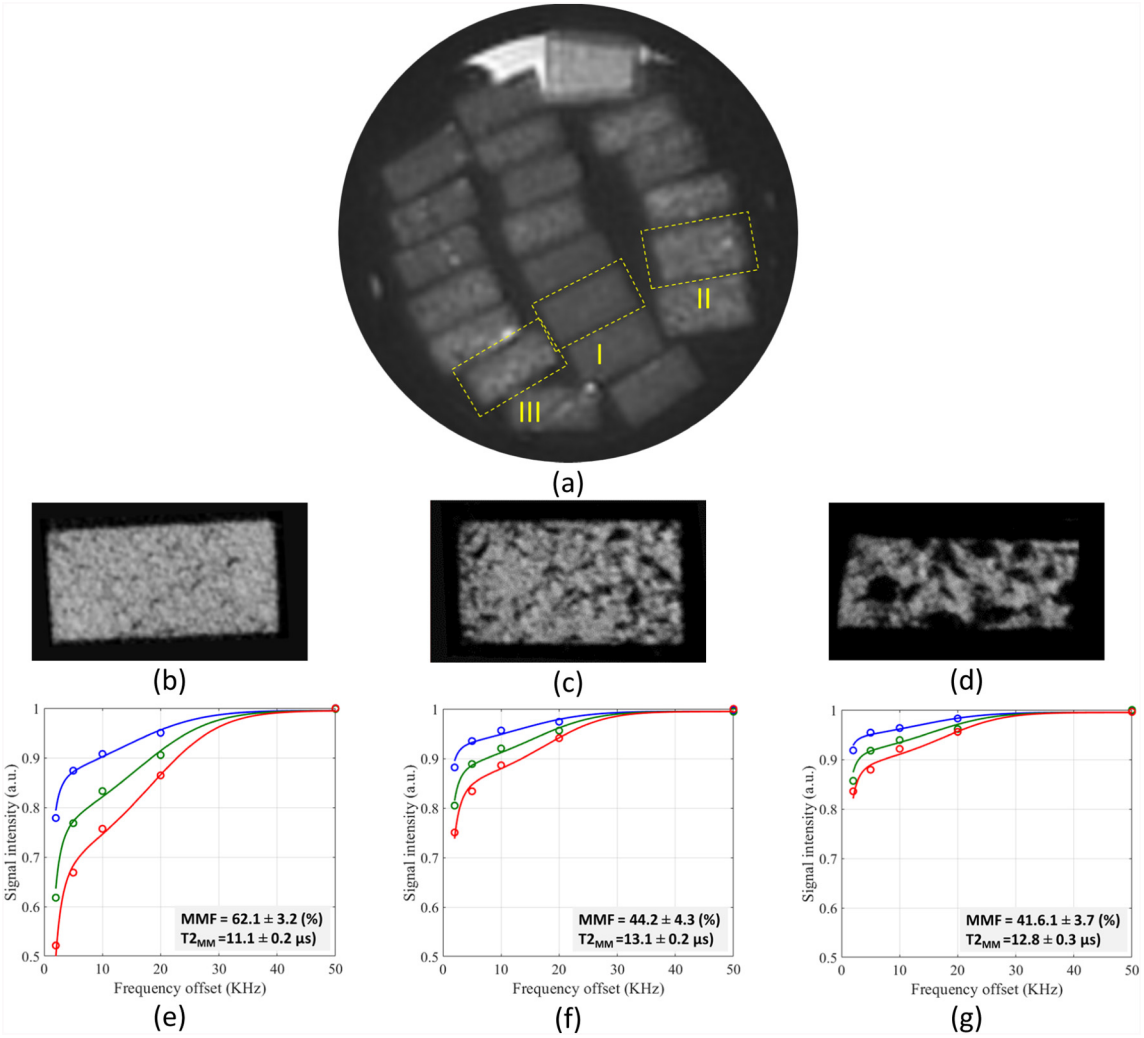

Fig. 2. UTE-MRI, μCT images, and MT-modeling results of three representative cortical bone strips harvested from different donors possessing three different levels of porosities. (a) UTE-MRI (TE = 0.032 ms) images of twenty cortical bone strips with approx. 4 × 2 mm cross-sections. Three of the cortical bone strips harvested from a 47-year-old male (I), a 57-year-old female (II), and a 91-year-old female (III) are indicated with yellow rectangles. A rubber reference was also scanned together with bone samples, showing with much brighter signal at the top of the syringe cross-section. (b), (c), and (d) Corresponding μCT images of cortical bone strips indicated as I, II, and III, respectively in Fig. 2(a). Average porosity was 5%, 33%, and 53% for specimens (b), (c), and (d), respectively. (e), (f), and (g) The two-pool MT modeling analyses for bone strips indicated in (a) as I, II, and III, respectively, using three pulse power levels (400° in blue, 600° in green, and 800° in red) and five frequency offsets (2, 5, 10, 20, 50 kHz). MMF and $T2_{MM}$ refer to macromolecular fraction and macromolecular T2, respectively.

and pore size), as well as between UTE-MRI measures and mechanical properties (Young's modulus, yield stress, ultimate stress, and failure energy). To understand the independent prediction level of mechanical properties by MMF, the correlation coefficients between MMF and mechanical properties were also calculated after adjusting for porosity and BMD variations. Correlations with *p*-values below 0.05 were considered significant. All MRI, microstructural, mechanical, and statistical measurements and models were performed using codes developed in-house in MATLAB (version 2017, The Mathworks Inc., Natick, MA, USA).

3. Results

Fig. 2a shows the UTE-MRI images in axial plane at the middle of twenty bone strips with 4 mm × 2 mm approximate cross-sections. Three representative cortical bone specimens harvested from three different donors (47-year-old male (I), 57-year-old female (II), and 91-year-old female (III)) are indicated by yellow rectangles. Fig. 3b-d present the corresponding μCT images of the same bone specimens with an average of 5%, 33%, and 53% porosity values, respectively. The two-pool MT modeling analyses for these bone strips are presented in Fig. 3e-g. MT modeling was performed for five off-resonance frequencies (2, 5, 10, 20, and 50 kHz) and three MT saturation pulse power levels, including 400°, 600°, and 800°, indicated with blue, green, and red lines, respectively. As expected, MMF was higher for specimens with lower porosity.

Pearson's correlation coefficients and statistical significance of UTE-MRI measures (T1, MMF, and $T2_{MM}$) with μCT measures (BMD, porosity, and pore size) and with mechanical properties (Young's modulus, yield stress, ultimate stress, and failure energy) are presented in Table 1. MMF showed significant strong correlations with the bone porosity (R = -0.72, $P < 0.01$) and BMD (R = +0.71, $P < 0.01$). Significant moderate correlation was found between MMF and pore size measured from μCT data (R = -0.61, $P < 0.01$). Young's modulus, yield stress, and ultimate stress demonstrated significant moderate correlations with MMF ($R = 0.60–0.61$, $P < 0.01$). T1 and $T2_{MM}$ demonstrated non-significant correlations with bone microstructural and mechanical properties. The correlations between mechanical properties and MMF were found to be poor and mostly nonsignificant after adjusting for porosity and BMD variations ($R = 0.13–0.22$,

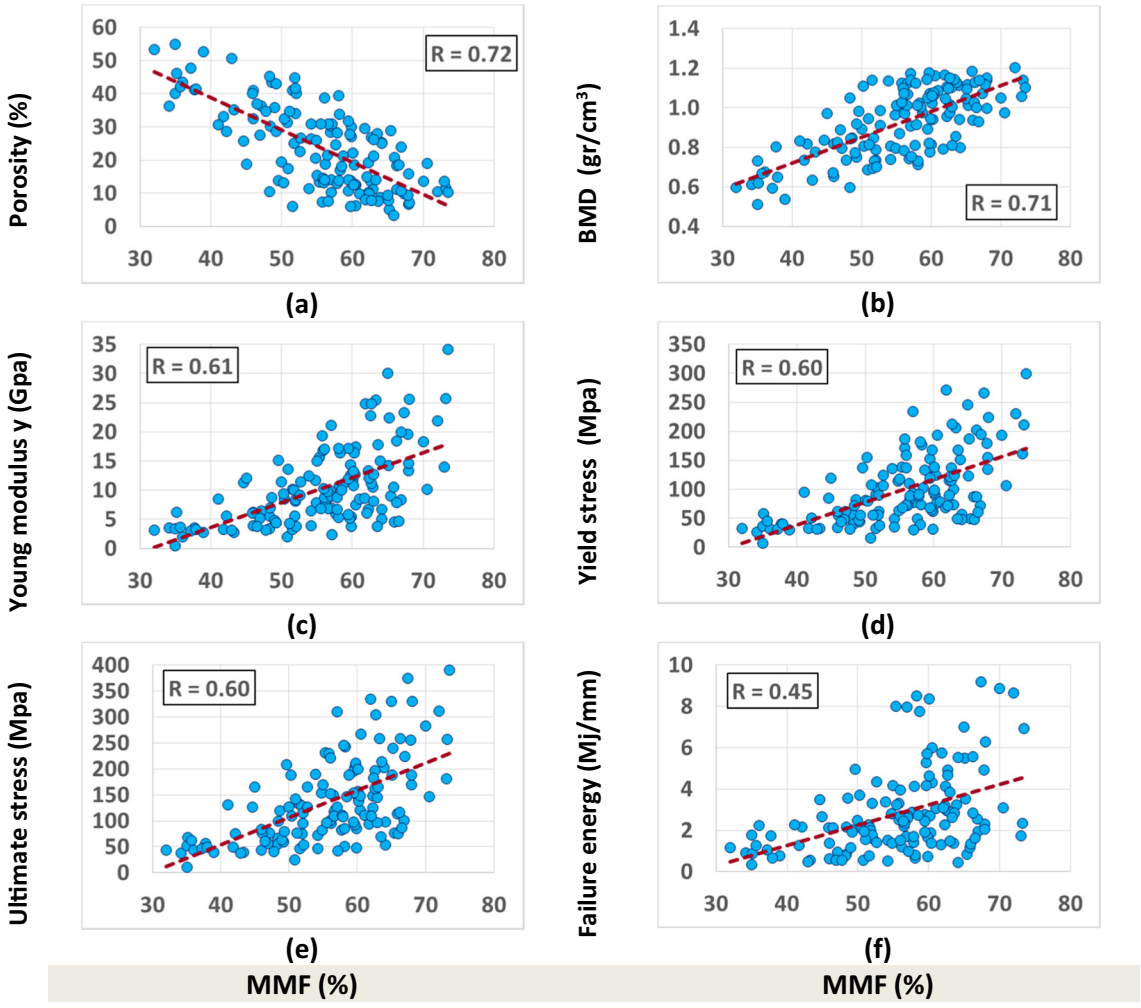

Fig. 3. Scatter plots and linear regression analyses with significant ($p < 0.01$) correlations of microstructural and mechanical properties on macromolecular fraction (MMF) for studied cortical bone strips. (a) μCT-porosity, (b) bone mineral density (BMD), (c) Young modulus, (d) yield stress, (e) ultimate stress, and (f) failure energy *versus* MMF.

$P = 0.01–0.15$).

Table 2 presents the Pearson's correlation coefficients and statistical significance between μCT measures and mechanical properties. Bone porosity and BMD both demonstrated significant strong correlations with Young modulus, yield stress, and ultimate stress ($R > 0.70$, $P < 0.01$). μCT-based pore size showed significant moderate correlations with aforementioned mechanical properties (R = -0.52 to −0.65, $P < 0.01$). The μCT correlations with mechanical properties were higher than the MMF correlations with mechanical properties for the studied specimens.

Fig. 3a and b depict the scatter plots and linear regressions of μCT-based bone porosity and BMD on the estimated MMF from MT modeling, respectively. Fig. 3c, d, e, and f, show the scatter plots and linear regressions of Young modulus, yield stress, ultimate stress, and failure

Table 2
Pearson's correlation coefficients between μCT-based microstructural measures and mechanical properties for 156 studied cortical bone strips.

	Young modulus	Yield stress	Ultimate stress	Failure energy
BMD	0.70 ($P < 0.01$)	0.74 ($P < 0.01$)	0.75 ($P < 0.01$)	0.52 ($P < 0.01$)
Porosity	−0.71 ($P < 0.01$)	−0.72 ($P < 0.01$)	−0.74 ($P < 0.01$)	−0.52 ($P < 0.01$)
Pore size	−0.61 ($P < 0.01$)	−0.65 ($P < 0.01$)	−0.67 ($P < 0.01$)	−0.52 ($P < 0.01$)

Table 1
Pearson's correlation coefficients between studied UTE-MRI measures and μCT results as well as mechanical properties for 156 studied cortical bone strips.

	BMD	Porosity	Pore size	Young modulus	Yield stress	Ultimate stress	Failure energy
T1	−0.10 ($P = 0.23$)	0.14 ($P = 0.12$)	0.11 ($P = 0.22$)	−0.10 ($P = 0.26$)	−0.10 ($P = 0.23$)	−0.11 ($P = 0.20$)	−0.12 ($P = 0.24$)
MMF	0.71 ($P < 0.01$)	−0.72 ($P < 0.01$)	−0.61 ($P < 0.01$)	0.61 ($P < 0.01$)	0.60 ($P < 0.01$)	0.60 ($P < 0.01$)	0.45 ($P < 0.01$)
$T2_{MM}$	−0.13 ($P = 0.14$)	0.11 ($P = 0.21$)	−0.04 ($P = 0.63$)	0.01 ($P = 0.94$)	−0.01 ($P = 0.89$)	0.00 ($P = 0.99$)	0.04 ($P = 0.84$)

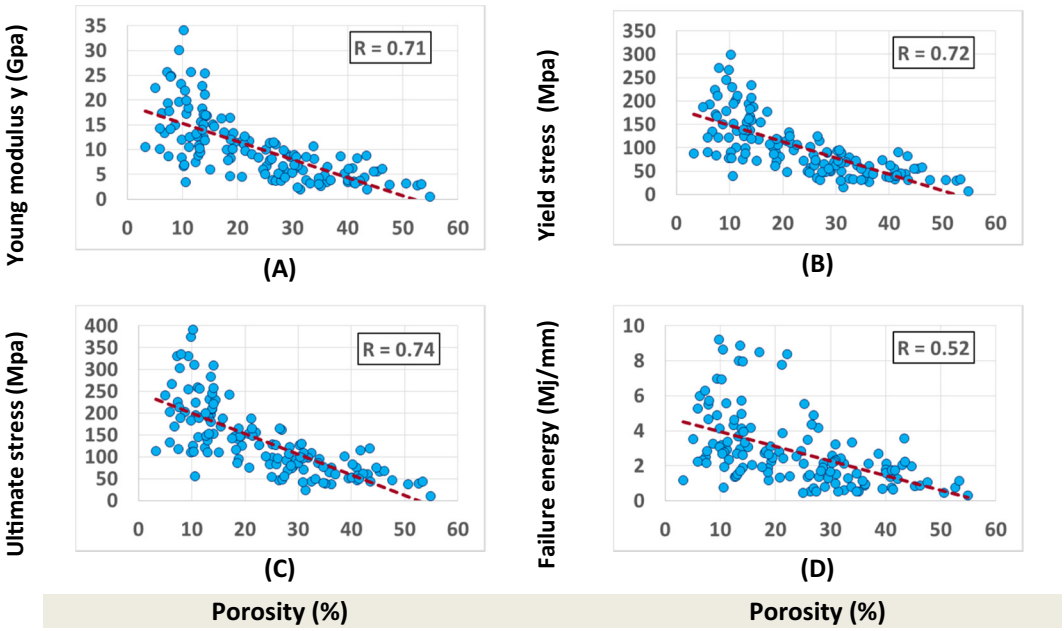

Fig. 4. Scatter plots and linear regression analyses of mechanical properties on μCT-based porosity for studied cortical bone strips. (a) Young modulus, (b) yield stress, (c) ultimate stress, and (d) failure energy *versus* μCT-based porosity.

energy on MMF, respectively.

Scatter plots and linear regressions of Young modulus, yield stress, ultimate stress, and failure energy on μ-CT based porosity are illustrated in Fig. 4a, b, c, and d, respectively.

4. Discussion

This study focused on recently developed UTE-MT-based measures of collagenous matrix for *ex vivo* assessment of cortical bone's mechanical properties. MMF from UTE-MT modeling techniques can provide an estimation of the collagen content in cortical bone (Ma et al., 2016a; Ma et al., 2017a; Ma et al., 2017b; Ramani et al., 2002). It is hypothesized that such estimation of the collagenous matrix content correlates with bone mechanical properties and can potentially help to improve the estimations of bone fracture risk in patients.

Previous MRI-based assessments of the mechanical properties of cortical bone have only focused on the water hydrogen pools. The pore water pool has been estimated for its potential correlation with mechanical properties. Fernandez et al. found significant inverse correlations between bone mechanical properties and total water content as measured with NMR spectroscopy in a limited number of specimens (n = 11, R = 0.72–0.77) (Fernández-Seara et al., 2004). Horch and Nyman et al. demonstrated direct significant correlations between estimated bound water pool from NMR spectroscopy and cortical bone mechanical properties (n = 18, R = 0.60, and n = 40, R = 0.82) (Nyman et al., 2008; Horch et al., 2011). They also showed significant negative correlations between pore water pool and mechanical properties (n = 18, R = 0.45 and n = 40, R = 0.78). Later, Horch et al. (Horch et al., 2012) used UTE-MRI for direct imaging of bound and pore water, and presented significant correlations with mechanical properties (n = 14, R = 0.68–0.83). Bae et al. presented significant correlations between bi-component T2* fitting results and the mechanical properties of human cortical bone (n = 44, R = 0.54) (Bae et al., 2012). Chang et al. found significant correlations between bone mechanical properties and MT ratio (n = 122, R = 0.55) (Chang et al., 2015b). Granke et al. reported significant correlations between bone NMR spectroscopy results of pore and bound water peaks with human bone fracture toughness (n = 62, R = 0.63) (Granke et al., 2015b). Manhard et al. investigated the correlations of bone fracture toughness and bending strength with direct MR imaging of pore and bound water (Manhard et al., 2016). They found significant correlation between bound water content and bone fracture toughness only for specimens from a male donor (n = 20, R = 0.51). They also reported significant correlations between bending strength and the bone's pore water and bound water contents (n = 40, R = 0.56–0.74).

This study was the first investigation to draw correlations between the parameters of bone mechanics and macromolecular fraction, obtained from a two-pool UTE-MT model, as an index of bone organic matrix density. UTE-MT modeling focuses on evaluation of the collagenous matrix of the bone for its potential applications in predicting bone mechanical properties. Estimated MMF in the scanned cortical bone specimens demonstrated significant moderate correlation with mechanical properties such as Young modulus, yield stress, and ultimate stress (R = 0.60–0.61, P < 0.01, Table 1, Fig. 3). As mentioned above, Chang et al. (Chang et al., 2015b) showed previously that the MTR from 2D radially acquired MT images correlated significantly with yield stress and ultimate stress. Although MTR and UTE-MT modeling share similar principles, describing collagen content based on MTR would be challenging since the ratios are hardware-dependent and vary significantly for different RF pulse powers and frequency offsets.

To validate the correlations between the UTE-MT measures and bone microstructural properties, μCT was used for bone porosity and BMD measurements. MMF showed strong negative correlation with bone porosity and showed strong positive correlation with BMD (Table 1, Fig. 3), which were in the range of previously reported correlations in tibial bone cross-sections imaged in clinically used knee coils (Jerban et al., 2019a; Jerban et al., 2019c). Other UTE-MRI techniques have also demonstrated good correlations with intracortical bone porosity measured with μCT. These techniques include bi-component T2* fitting (Bae et al., 2012), tri-component T2* analysis by modeling fat signal (Lu et al., 2019), dual-echo UTE imaging (*i.e.*, porosity index) (Rajapakse et al., 2015), T1-based decomposition of total water signal (Rad et al., 2011; Abbasi-Rad and Saligheh Rad, 2017), and direct pore water imaging after nulling bound water (Manhard et al., 2014; Li et al., 2014; Granke et al., 2015b).

The mechanical properties of the cortical bone specimens showed higher correlations with μCT-based measures compared with UTE-MT properties. Moreover, the correlations between MMF and mechanical

properties after adjusting for porosity and BMD variations were poor (R = 0.13–0.22). This can be true for healthy bone specimens and for those with osteoporotic disease, where the ratio between bone mineral and organic matrix remains approximately constant. The higher resolution of μCT data, which was more than twenty times the MRI resolution, could also result in higher correlations between μCT and mechanical properties. However, such resolutions may not be achievable *in vivo* for x-ray-based techniques. Nevertheless, in bone diseases such as osteomalacia (Bhan et al., 2018; Becker, 2005) and bone stress injuries (Jerban et al., 2018; Kijowski et al., 2012), where the bone mineral and bone organic matrix vary independently, utilizing the UTE-MT-MRI technique could improve the sensitivity and specificity of diagnosis.

The results of this study suggest that MMF from UTE-MT modeling is a useful and promising index for evaluating mechanical and microstructural properties of human cortical for specimens from donors with no known bone disease. This MRI-based technique is non-invasive, x-ray-free, and, importantly, translatable to *in vivo* and clinical studies. Focusing on the collagen matrix of the bone besides the mineral density may be valuable for improving estimation of bone fracture risk.

This study was limited in some aspects. First, this study was performed on *ex vivo* bone specimens cut from pure cortical bone layers, where low bone marrow and no surrounding muscles were present. Future *in vivo* studies of two-pool UTE-MT modeling may not be able to predict bone's mechanical properties as presented here due to penetration of bone marrow fat into bone pores of the cortex. Therefore, the consideration of three-pool UTE-MT modeling is a promising path for future studies. An additional alternative for future *in vivo* studies would be different fat suppression techniques followed by two-pool MT modeling. Optimizing fat suppression to minimize the contamination on the water proton signal would be a crucial prerequisite for this approach (Ma et al., 2019; Jang et al., 2019). Subject's motion during scan and temperature differences (Jerban et al., 2019d) are other challenging factors that need be addressed before translating this technique to clinical studies. The second limitation of this study was the long scan time (70 min approximately). Although the *in vivo* scans will be in lower resolution and therefore require much decreased scan time (*e.g.*, 35 min), it may be difficult for patients to remain still for this duration of time. Employing different accelerating techniques, such as stretching the cones readout trajectory, could be used to accelerate and optimize the 3D-UTE-Cones sequences with negligible errors (Wan et al., 2019). Another way to reduce the total scan time is to eliminate T1 measurement, which comprises more than half of the total scan time. Investigating T1's age dependency in future *ex vivo* and *in vivo* studies may help generate an age-dependent T1 chart which could then be used as the input in the presented MT modeling technique. A third limitation of this investigation was that the studied mechanical properties were limited to tensile failure properties obtained from 4-point bending tests. Organic bone matrix may be more determinative in predicting the impact failure phenomena that can be estimated using bone toughness tests to estimate the crack initiation resistance and crack progress resistance (Granke et al., 2015b). Fourth, the studied cortical bone strips were harvested from long bone midshafts; however, most osteoporotic bone fractures in patients occur in the proximal femoral. Thus, a follow up *ex vivo* study should be performed to investigate UTE-MT analyses on the femoral neck and its correlations with mechanical properties.

5. Conclusion

Two-pool UTE-MT modeling was investigated for its capability to assess mechanical properties of cortical bone in an *ex vivo* study performed on bone strips from human tibial and femoral midshafts. MMF obtained from MT modeling, as a quantification of collagenous matrix content, showed significant moderate correlations with Young's modulus, yield stress, and ultimate stress, measured with 4-point bending tests. MMF also showed strong correlations with μCT-based bone porosity and BMD. This study highlighted UTE-MT MRI techniques as a useful method to assess cortical bone mechanical properties and intracortical bone microstructure, which may be useful in future clinical studies for fracture risk estimation.

Conflict of interest statement

The authors have no conflicts of interest to declare.

Transparency document

The Transparency document associated with this article can be found, in online version.

Acknowledgements

The authors acknowledge grant support from NIH (1R21AR073496, R01AR068987, 1R01AR062581-01A1) and VA Clinical Science and Rehabilitation R&D (I01CX001388, I01RX002604). The authors also declare that Jiang Du and Yajun Ma have been inventors in two related US patents regarding UTE-MT modeling and T1 measurement techniques (US20190142297, US20190079154A1).

References

Abbasi-Rad, S., Saligheh Rad, H., 2017. Quantification of human cortical bone bound and free water in vivo with ultrashort echo time MR imaging: a model-based approach. Radiology 000, 160780. https://doi.org/10.1148/radiol.2016160780.

ASTM, 2011. Standard Test Methods for Flexural Properties of Unreinforced and Reinforced Plastics and Electrical Insulating Materials 1, Annu. B. ASTM Stand. pp. 1–11. https://doi.org/10.1520/D0790-10.

ASTM, 2015. ASTM C1674–11 Standard Test Method for Flexural Strength of Advanced Ceramics with Engineered Porosity (Honeycomb Cellular Channels) at Ambient Temperatures, Annu. B. ASTM Stand. I. pp. 10. https://doi.org/10.1520/C1674-11.2.

Bae, W.C., Chen, P.C., Chung, C.B., Masuda, K., D'Lima, D., Du, J., 2012. Quantitative ultrashort echo time (UTE) MRI of human cortical bone: correlation with porosity and biomechanical properties. J. Bone Miner. Res. 27, 848–857. https://doi.org/10.1002/jbmr.1535.

Baratta, F.I., 1982. Requirements for flexure testing of brittle materials. Army Mater. Mech. Res. Cent. 46. https://doi.org/10.1520/STP35245S.

Bashoor-Zadeh, M., Baroud, G., Bohner, M., 2010. Geometric analysis of porous bone substitutes using micro-computed tomography and fuzzy distance transform. Acta Biomater. 6, 864–875. https://doi.org/10.1016/j.actbio.2009.08.007.

Becker, C., 2005. In: Kleerekoper, M., Siris, E.S. (Eds.), 28 - Osteomalacia. Academic Press, Burlington, pp. 141–146. https://doi.org/10.1016/B978-012088569-5/50029-2. M.B.T.-T.B. and M.M. (Second E. McClung.

Bhan, A., Qiu, S., Rao, S.D., 2018. Bone histomorphometry in the evaluation of osteomalacia. Bone Reports 8, 125–134. https://doi.org/10.1016/j.bonr.2018.03.005.

Bigley, R.F., Gibeling, J.C., Stover, S.M., Hazelwood, S.J., Fyhrie, D.P., Martin, R.B., 2008a. Volume effects on yield strength of equine cortical bone. J. Mech. Behav. Biomed. Mater. 1, 295–302. https://doi.org/10.1016/j.jmbbm.2007.11.001.

Bigley, R.F., Gibeling, J.C., Stover, S.M., Hazelwood, S.J., Fyhrie, D.P., Martin, R.B., 2008b. Volume effects on fatigue life of equine cortical bone. J. Mech. Behav. Biomed. Mater. 1, 295–302. https://doi.org/10.1016/j.jmbbm.2007.11.001.

Carl, M., Bydder, G.M., Du, J., 2015. UTE imaging with simultaneous water and fat signal suppression using a time-efficient multispoke inversion recovery pulse sequence. Magn. Reson. Med. 76, 577–582. https://doi.org/10.1002/mrm.25823.

Chang, E.Y., Du, J., Chung, C.B., 2015a. UTE imaging in the musculoskeletal system. J. Magn. Reson. Imaging 41, 870–883. https://doi.org/10.1002/jmri.24713.

Chang, E.Y., Bae, W.C., Shao, H., Biswas, R., Li, S., Chen, J., Patil, S., Healey, R., Lima, D.D.D., Chung, C.B., Du, J., 2015b. Ultrashort echo time magnetization transfer (UTE-MT) imaging of cortical bone. NMR Biomed. 28, 873–880. https://doi.org/10.1002/nbm.3316.

Darabi, A., Chandelier, F., Baroud, G., 2007. Morphometric analysis of trabecular bone thickness using different algorithms. Can. J. Electr. Comput. Eng. 32, 157–163. https://doi.org/10.1109/CJECE.2007.4413127.

Diaz, E., Chung, C.B., Bae, W.C., Statum, S., Znamirowski, R., Bydder, G.M., Du, J., 2012. Ultrashort echo time spectroscopic imaging (UTESI): an efficient method for quantifying bound and free water. NMR Biomed. 25, 161–168. https://doi.org/10.1002/nbm.1728.

Du, J., Bydder, G.M., 2013. Qualitative and quantitative ultrashort-TE MRI of cortical bone. NMR Biomed. 26, 489–506. https://doi.org/10.1002/nbm.2906.

Du, J., Carl, M., Bydder, M., Takahashi, A., Chung, C.B., Bydder, G.M., 2010. Qualitative and quantitative ultrashort echo time (UTE) imaging of cortical bone. J. Magn. Reson. 207, 304–311. https://doi.org/10.1016/j.jmr.2010.09.013.

Fernández-Seara, M.A., Wehrli, S.L., Takahashi, M., Wehrli, F.W., 2004. Water content predicts bone mineral density and mechanical properties. J. Bone Joint Surg. Am. 19, 289–295. https://doi.org/10.1359/JBMR.0301227.

Granke, M., Does, M.D., Nyman, J.S., 2015a. The role of water compartments in the material properties of cortical bone. Calcif. Tissue Int. 97, 292–307. https://doi.org/10.1007/s00223-015-9977-5.

Granke, M., Makowski, A.J., Uppuganti, S., Does, M.D., Nyman, J.S., 2015b. Identifying novel clinical surrogates to assess human bone fracture toughness. J. Bone Miner. Res. 30, 1290–1300. https://doi.org/10.1002/jbmr.2452.

Gurney, P.T., Hargreaves, B.A., Nishimura, D.G., 2006. Design and analysis of a practical 3D cones trajectory. Magn. Reson. Med. 55, 575–582. https://doi.org/10.1002/mrm.20796.

Hammant, B., 1971. The use of 4-point loading tests to determine mechanical properties. Composites 2, 246–249. https://doi.org/10.1016/0010-4361(71)90154-6.

Hildebrand, T., Rüegsegger, P., 1997. A new method for the model-independent assessment of thickness in three-dimensional images. J. Microsc. 185, 67–75. https://doi.org/10.1046/j.1365-2818.1997.1340694.x.

Horch, R.A., Gochberg, D.F., Nyman, J.S., Does, M.D., 2011. Non-invasive predictors of human cortical bone mechanical properties: T2-discriminated 1H NMR compared with high resolution X-ray. PLoS One 6, 1–5. https://doi.org/10.1371/journal.pone.0016359.

Horch, R.A., Gochberg, D.F., Nyman, J.S., Does, M.D., 2012. Clinically compatible MRI strategies for discriminating bound and pore water in cortical bone. Magn. Reson. Med. 68, 1774–1784. https://doi.org/10.1002/mrm.24186.

Jang, H., Lu, X., Carl, M., Searleman, A.C., Jerban, S., Ma, Y., Drygalski, A. von, Chang, E.Y., Du, J., 2018. True phase quantitative susceptibility mapping using continuous single-point imaging: a feasibility study. Magn. Reson. Med. 1–8. https://doi.org/10.1002/mrm.27515.

Jang, H., Carl, M., Ma, Y., Jerban, S., Guo, T., Zhao, W., Chang, E.Y., Du, J., 2019. Fat suppression for ultrashort echo time imaging using a single point Dixon method. NMR Biomed. e4069. https://doi.org/10.1002/nbm.4069.

Jerban, S., Ma, Y., Nazaran, A., Dorthe, E.W., Cory, E., Carl, M., D'Lima, D., Sah, R.L., Chang, E.Y., Du, J., D'Lima, D., Sah, R.L., Chang, E.Y., Du, J., 2018. Detecting stress injury (fatigue fracture) in fibular cortical bone using quantitative ultrashort echo time-magnetization transfer (UTE-MT): an ex vivo study. NMR Biomed. 31, e3994. https://doi.org/10.1002/nbm.3994.

Jerban, S., Ma, Y., Wan, L., Searleman, A.C., Jang, H., Sah, R.L., Chang, E.Y., Du, J., 2019a. Collagen proton fraction from ultrashort echo time magnetization transfer (UTE-MT) MRI modelling correlates significantly with cortical bone porosity measured with micro-computed tomography (μCT). NMR Biomed. 32, 1–10. https://doi.org/10.1002/nbm.4045.

Jerban, S., Lu, X., Jang, H., Ma, Y., Namiranian, B., Le, N., Li, Y., Chang, E.Y., Du, J., 2019b. Significant correlations between human cortical bone mineral density and quantitative susceptibility mapping (QSM) obtained with 3D Cones ultrashort echo time magnetic resonance imaging (UTE-MRI). Magn. Reson. Imaging. https://doi.org/10.1016/j.mri.2019.06.016.

Jerban, S., Ma, Y., Wong, J.H., Nazaran, A., Searleman, A., Wan, L., Williams, J., Du, J., Chang, E.Y., 2019c. Ultrashort echo time magnetic resonance imaging (UTE-MRI) of cortical bone correlates well with histomorphometric assessment of bone microstructure. Bone 123, 8–17. https://doi.org/10.1016/j.bone.2019.03.013.

Jerban, S., Szeverenyi, N., Ma, Y., Guo, T., Namiranian, B., To, S., Jang, H., Chang, Eric Y., Du, J., 2019d. Ultrashort echo time MRI (UTE-MRI) quantifications of cortical bone varied significantly at body temperature compared with room temperature. Investig. Magn. Reson. Imaging 23 (3), 200–206. https://doi.org/10.13104/imri.2019.23.3.200.

Khandaker, M., Ekwaro-Osire, S., 2013. Weibull analysis of fracture test data on bovine cortical bone: influence of orientation. Int. J. Biomater. 2013. https://doi.org/10.1155/2013/639841.

Kijowski, R., Choi, J., Shinki, K., Del Rio, A.M., De Smet, A., 2012. Validation of MRI classification system for tibial stress injuries. Am. J. Roentgenol. 198, 878–884. https://doi.org/10.2214/AJR.11.6826.

Koudelka, P., Jiroušek, O., Valach, J., 2011. Determination of mechanical properties of materials with complex inner structure using microstructural models. Mach. Technol. Mater. 1, 39–42. http://mech-ing.com/journal/3-2011.html.

Li, C., Seifert, A.C., Rad, H.S., a Bhagat, Y., Rajapakse, C.S., Sun, W., Lam, S.C.B., Wehrli, F.W., 2014. Cortical bone water concentration: dependence of MR imaging measures on age and pore volume fraction. Radiology 272, 796–806. https://doi.org/10.1148/radiol.14132585.

Lu, X., Jerban, S., Wan, L., Ma, Y., Jang, H., Le, N., Yang, W., Chang, E.Y., Du, J., 2019. Three dimensional ultrashort Echo time imaging with tri-component analysis for human cortical bone. Magn. Reson. Med. 82, 348–355. https://doi.org/10.1002/mrm.27718.

Ma, Y., Shao, H., Du, J., Chang, E.Y., 2016a. Ultrashort echo time magnetization transfer (UTE-MT) imaging and modeling: magic angle independent biomarkers of tissue properties. NMR Biomed. 29, 1546–1552. https://doi.org/10.1002/nbm.3609.

Ma, Y., Chang, E.Y., Bydder, G.M., Du, J., 2016b. Can ultrashort-TE (UTE) MRI sequences on a 3-T clinical scanner detect signal directly from collagen protons: freeze–dry and D2O exchange studies of cortical bone and Achilles tendon specimens. NMR Biomed. 29, 912–917. https://doi.org/10.1002/nbm.3547.

Ma, Y., Chang, E.Y., Carl, M., Du, J., 2017a. Quantitative magnetization transfer ultrashort echo time imaging using a time-efficient 3D multispoke Cones sequence. Magn. Reson. Med. 00, 1–9. https://doi.org/10.1002/mrm.26716.

Ma, Y., Tadros, A., Du, J., Chang, E.Y., 2017b. Quantitative two-dimensional ultrashort echo time magnetization transfer (2D UTE-MT) imaging of cortical bone. Magn. Reson. Med. https://doi.org/10.1002/mrm.26846.

Ma, Y., Zhu, Y., Lu, X., Carl, M., Chang, E.Y., Du, J., 2017c. Short T 2 imaging using a 3D double adiabatic inversion recovery prepared ultrashort echo time cones (3D DIR-UTE-Cones) sequence. Magn. Reson. Med. 00, 1–9. https://doi.org/10.1002/mrm.26908.

Ma, Y., Lu, X., Carl, M., Zhu, Y., Szeverenyi, N.M., Bydder, G.M., Chang, E.Y., Du, J., 2018. Accurate T 1 mapping of short T 2 tissues using a three-dimensional ultrashort echo time cones actual flip angle imaging-variable repetition time (3D UTE-Cones AFI-VTR) method. Magn. Reson. Med. 00, 1–11. https://doi.org/10.1002/mrm.27066.

Ma, Y., Jerban, S., Jang, H., Chang, E.Y., Du, J., 2019. Fat suppression for ultrashort echo time imaging using a novel soft-hard composite radiofrequency pulse. Magn. Reson. Med. 00, 1–10. https://doi.org/10.1002/mrm.27885.

Manhard, M.K., Horch, R.A., Harkins, K.D., Gochberg, D.F., Nyman, J.S., Does, M.D., 2014. Validation of quantitative bound- and pore-water imaging in cortical bone. Magn. Reson. Med. 71, 2166–2171. https://doi.org/10.1002/mrm.24870.

Manhard, M.K., Horch, R.A., Gochberg, D.F., Nyman, J.S., Does, M.D., 2015. In vivo quantitative MR imaging of bound and pore water in cortical bone. Radiology 277, 221–230.

Manhard, M.K., Uppuganti, S., Granke, M., Gochberg, D.F., Nyman, J.S., Does, M.D., 2016. MRI-derived bound and pore water concentrations as predictors of fracture resistance. Bone 87, 1–10. https://doi.org/10.1016/j.bone.2016.03.007.

Manhard, M.K., Nyman, J.S., Does, M.D., 2017. Advances in imaging approaches to fracture risk evaluation. Transl. Res. 181, 1–14. https://doi.org/10.1016/j.trsl.2016.09.006.

Moser, E., Rejnmark, L., Sikjaer, T., Mosekilde, L., Amstrup, A.K., Jakobsen, N.F.B., 2015. Association between bone indices assessed by DXA, HR-pQCT and QCT scans in postmenopausal women. J. Bone Miner. Metab. 34, 638–645. https://doi.org/10.1007/s00774-015-0708-9.

Nazaran, A., Carl, M., Ma, Y., Jerban, S., Lu, X., Du, J., Chang, E.Y., 2017. Three-dimensional adiabatic inversion recovery prepared ultrashort echo time cones (3D IR-UTE-Cones) imaging of cortical bone in the hip. Magn. Reson. Imaging. https://doi.org/10.1016/j.mri.2017.07.012. In Press.

Nyman, J.S., Ni, Q., Nicolella, D.P., Wang, X., 2008. Measurements of mobile and bound water by nuclear magnetic resonance correlate with mechanical properties of bone. Bone 42, 193–199. https://doi.org/10.1016/j.bone.2007.09.049.

Quinn, J.B., Quinn, G.D., 2010. A practical and systematic review of Weibull statistics for reporting strengths of dental materials. Dent. Mater. 26, 135–147. https://doi.org/10.1016/j.dental.2009.09.006.

Rad, H.S., Lam, S.C.B., Magland, J.F., Ong, H., Li, C., Song, H.K., Love, J., Wehrli, F.W., 2011. Quantifying cortical bone water in vivo by three-dimensional ultra-short echo-time MRI. NMR Biomed. 24, 855–864. https://doi.org/10.1002/nbm.1631.

Rajapakse, C.S., Bashoor-Zadeh, M., Li, C., Sun, W., Wright, A.C., Wehrli, F.W., 2015. Volumetric cortical bone porosity assessment with MR imaging: validation and clinical feasibility. Radiology 276, 526–535. https://doi.org/10.1148/radiol.15141850.

Ramani, A., Dalton, C., Miller, D.H., Tofts, P.S., Barker, G.J., 2002. Precise estimate of fundamental in-vivo MT parameters in human brain in clinically feasible times. Magn. Reson. Imaging 20, 721–731. https://doi.org/10.1016/S0730-725X(02)00598-2.

Seifert, A.C., Wehrli, F.W., 2016. Solid-state quantitative 1H and 31P MRI of cortical bone in humans. Curr. Osteoporos. Rep. 1–10. https://doi.org/10.1007/s11914-016-0307-2.

Springer, F., Martirosian, P., Machann, J., Schwenzer, N.F., Claussen, C.D., Schick, F., 2009. Magnetization transfer contrast imaging in bovine and human cortical bone applying an ultrashort echo time sequence at 3 Tesla. Magn. Reson. Med. 61, 1040–1048. https://doi.org/10.1002/mrm.21866.

Tyler, D.J., Robson, M.D., Henkelman, R.M., Young, I.R., Bydder, G.M., 2007. Magnetic resonance imaging with ultrashort TE (UTE) PULSE sequences: technical considerations. J. Magn. Reson. Imaging 25, 279–289. https://doi.org/10.1002/jmri.20851.

Wan, L., Zhao, W., Ma, Y., Jerban, S., Searleman, A.C., Carl, M., Chang, E.Y., Tang, G., Du, J., 2019. Fast quantitative three-dimensional ultrashort echo time (UTE) magnetic resonance imaging of cortical bone using extended cones sampling. Magn. Reson. Med. https://doi.org/10.1002/mrm.27715.

Wehrli, F.W., 2013. Magnetic resonance of calcified tissues. J. Magn. Reson. 229, 35–48. https://doi.org/10.1016/j.jmr.2012.12.011.

Weibull, W., 1939. A Statistical Theory of the Strength of Materials.

Zhao, X., Song, H.K., Seifert, A.C., Li, C., Wehrli, F.W., 2017. Feasibility of assessing bone matrix and mineral properties in vivo by combined solidstate 1H and 31P MRI. PLoS One 12, 1–16. https://doi.org/10.1371/journal.pone.0173995.